

## Topodiagnostic implications of hemiataxia: An MRI-based brainstem mapping analysis

Juergen J. Marx,<sup>a,\*</sup> Gian D. Iannetti,<sup>d</sup> Frank Thömke,<sup>a</sup> Sabine Fitzek,<sup>e</sup> Francesca Galeotti,<sup>c</sup> Andrea Truini,<sup>c</sup> Peter Stoeter,<sup>b</sup> Marianne Dieterich,<sup>a</sup> Hanns C. Hopf,<sup>a</sup> and Giorgio Cruccu<sup>c</sup>

<sup>a</sup>Department of Neurology, Johannes Gutenberg-University Mainz, Langenbeckstr. 1, D-55101 Mainz, Germany

<sup>b</sup>Department of Neuroradiology, Johannes Gutenberg-University Mainz, Germany

<sup>c</sup>Department of Neurological Sciences, La Sapienza University, Rome, Italy

<sup>d</sup>Department of Physiology, Anatomy and Genetics, University of Oxford, UK

<sup>e</sup>Department of Neurology, DRK Hospital, Berlin-Köpenick, Germany

Received 8 June 2007; revised 23 August 2007; accepted 3 October 2007

Available online 16 October 2007

The topodiagnostic implications of hemiataxia following lesions of the human brainstem are only incompletely understood. We performed a voxel-based statistical analysis of lesions documented on standardised MRI in 49 prospectively recruited patients with acute hemiataxia due to isolated unilateral brainstem infarction. For statistical analysis individual MRI lesions were normalised and imported in a three-dimensional voxel-based anatomical model of the human brainstem. Statistical analysis revealed hemiataxia to be associated with lesions of three distinct brainstem areas. The strongest correlation referred to ipsilateral rostral and dorsolateral medullary infarcts affecting the inferior cerebellar peduncle, and the dorsal and ventral spinocerebellar tracts. Secondly, lesions of the ventral pontine base resulted in contralateral limb ataxia, especially when ataxia was accompanied by motor hemiparesis. In patients with bilateral hemiataxia, lesions were located in a paramedian region between the upper pons and lower midbrain, involving the decussation of dentato-rubro-thalamic tracts. We conclude that ataxia following brainstem infarction may reflect three different pathophysiological mechanisms. (1) Ipsilateral hemiataxia following dorsolateral medullary infarctions results from a lesion of the dorsal spinocerebellar tract and the inferior cerebellar peduncle conveying afferent information from the ipsilateral arm and leg. (2) Pontine lesions cause contralateral and not bilateral ataxia presumably due to major damage to the descending corticopontine projections and pontine base nuclei, while already crossed pontocerebellar fibres are not completely interrupted. (3) Finally, bilateral ataxia probably reflects a lesion of cerebellar outflow on a central, rostral pontomesencephalic level.

© 2007 Elsevier Inc. All rights reserved.

**Keywords:** Brain stem; Ataxia; Brain mapping; MRI

### Introduction

Limb ataxia is a common disabling symptom in patients with cerebellar or brainstem ischaemia. It is known to be a frequent sign of typical dorsolateral medullary infarction (Rondot, 1969). While the topography in accompanying symptoms such as gait ataxia, dysphagia and different sensory patterns has been studied extensively, the topodiagnostic implications of acute hemiataxia have not received as much attention (Kim, 2003; Sacco et al., 1993). Limb ataxia is, however, also reported in patients with pure pontine ischaemia (Kumral et al., 2002; Schmahmann et al., 2004b). Even though neuroradiological imaging considerably advanced in the last decade, the topodiagnostic value of limb ataxia as a sign of brainstem dysfunction and the potential role of several structures, especially descending corticopontine fibre tracts, various pontine nuclei and pontocerebellar projections remains to be elucidated. Anatomical-functional correlation studies are particularly difficult in the brainstem due to the close proximity of nuclei and fibre tracts and the limited spatial resolution of the methods to date complicate reliable allocations of activations in functional magnetic resonance imaging (fMRI) or positron emission tomography (PET). Classical anatomical-functional correlation studies using post-mortem specimens or neuroimaging are, however, mostly anecdotal and based on a restricted number of samples providing qualitative rather than quantitative and statistically supported results.

In order to investigate the anatomical brainstem structures responsible for limb ataxia we analysed the topography of MRI lesions in prospectively recruited patients with hemiataxia following acute brainstem infarction. MRI scans were imported and normalised into a voxel-based model of the human brainstem with statistical analysis of lesion location. This new approach to three-dimensional brainstem mapping proved to be useful in earlier anatomical-functional correlation studies (Cruccu et al., 2005; Marx et al., 2005).

\* Corresponding author. Fax: +49 6131 173271.

E-mail address: [marx@neurologie.klinik.uni-mainz.de](mailto:marx@neurologie.klinik.uni-mainz.de) (J.J. Marx).

Available online on ScienceDirect ([www.sciencedirect.com](http://www.sciencedirect.com)).

## Patients and methods

Over a 3-year period we prospectively recruited 362 consecutive patients with acute signs and symptoms of vertebrobasilar ischaemia at two European neurological institutions with a special interest in brain stem dysfunction: the Department of Neurology, Johannes Gutenberg-University Mainz, Germany, and the Department of Neurological Sciences, La Sapienza University of Rome, Italy. Inclusion criteria were acute ocular motor disorders, cranial nerve dysfunction and limb or gait ataxia as indicators of acute vertebrobasilar dysfunction. All patients had magnetic resonance imaging (MRI) following a standardised protocol (see below). All patients with multiple brain stem lesions or additional cerebellar lesions were excluded from the mapping analysis.

Approval of the study was granted by the two local university ethics committees, and patients gave informed consent to the procedures.

### Clinical investigations

Detailed clinical examination was done within 24 h after onset of symptoms by two independent neurologists. For investigation of clinical limb ataxia we applied standard knee–tibia and finger–nose tests. Patients qualified for the mapping analysis, when limb ataxia was counted at least “2” in one of the two tests according to the criteria of the International Cooperative Ataxia Rating Scale (Trouillas et al., 1997). This corresponded to a lowering of the heel jerkily in the axis or a segmented movement in at least 2 phases and/or at least moderate dysmetria in reaching the nose with the finger. Pure lateropulsion, abnormal spread of feet or impaired walking capacities without limb ataxia were exclusion criteria for further mapping analysis. According to the NIH Stroke Scale, ataxia with accompanying motor paresis was only scored if it was present out of proportion to weakness (Brott et al., 1989). We used standard clinical tests to investigate for additional central motor hemiparesis. Muscle force in the distal and proximal upper and lower limbs was graded according to the standard Medical Research Council scale (MRC grades 0–5; grade 0 reflecting complete paresis and grade 5 full muscle power), and the presence or absence of pyramidal signs (drift of lifted limb, hyperreflexia, extensor plantar response, spasticity). To further investigate corticospinal tract involvement, MEPs were recorded in every patient who showed hemiataxia and

clinical signs suspicious of pyramidal tract dysfunction within 1 week after onset of symptoms. We used a circular coil (mean diameter of 9 cm, peak magnetic field 2.0 T, Magstim 200S, Novametrix, UK) for stimulation. Electromyographic recordings were taken bilaterally from upper and lower limb muscles using standard procedures (Urban et al., 1996). Absolute values for latency, amplitude, central conduction time, and side differences were evaluated according to our previously reported normal values (Urban et al., 2001). If clinical and electrophysiological signs of corticospinal tract involvement were present additionally to limb ataxia, this was defined as “ataxic hemiparesis.”

Patients were grouped according to the presence of uni- or bilateral limb ataxia and according to the affection of arm, leg or both limbs. Patients were excluded from the analysis, if severe hemiparesis did not allow proper examination for accompanying limb ataxia.

Patients with clinical hemiataxia (s.a.) were checked for additional clinical signs, especially the presence of sensory deficits in light/pressure touch or pain/temperature sensation (by use of standard semi-quantitative clinical tests and somatosensory evoked potentials of the tibial and median nerve), body lateropulsion, vestibular signs and ocular motor disorders. For investigation of subclinical ocular motor symptoms in 43 of the 49 patients electrooculography including caloric vestibular testing was applied. The remaining six patients were unable to perform the testing procedure due to the severity of neurological impairment.

### MR acquisition

As soon as patients could tolerate the longer lasting MR scans (mean: 6 days after the onset of symptoms), they underwent a standard MR brain study, followed by a focussed brainstem investigation. The MR scans were acquired using 1.5-T superconducting systems (Magnetom Vision, Siemens, Erlangen, Germany, and Philips Gyroscan, Best, The Netherlands). High-resolution T1- and T2-weighted brainstem images before and after intravenous gadolinium, were collected from all patients. To ensure standardised imaging slice orientation was parallel (sagittal sections) and perpendicular (axial sections) to the sagittal brainstem cuts of the stereotactic anatomical atlas of Schaltenbrand and Wahren (1977) (Fig. 1A); the slice thickness was 3 mm over a  $256 \times 256$  matrix. In about half of the patients biplanar EPI-T2 and

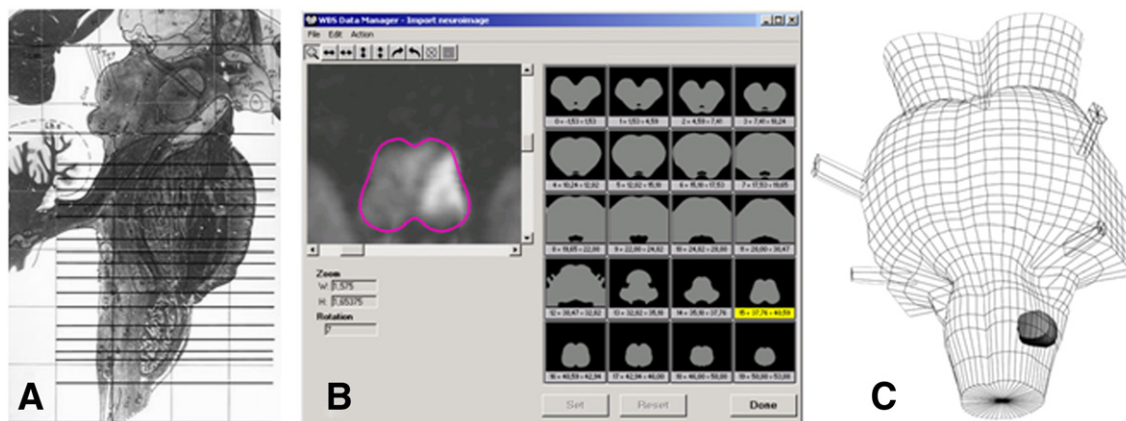


Fig. 1. MRI acquisition and lesion import. (A) Sagittal view of the brainstem according to the anatomical atlas of Schaltenbrand and Wahren (1977). Orientation of MRI scans was parallel and perpendicular to the axial slices shown. (B) Computer-based lesion identification, normalisation and import. (C) Example of a medullary lesion after import in the 3D voxel-based anatomical model.

Table 1

No.	Limb	Ataxia	Hemip	Latero	Pain/Temperature	Touch	Ocular motor disorders	Others	Lesion
1	A+L	Ipsi	No	Ipsi	Contra	No	Saccadic pursuit to R+L	Horner R, vail paresis R	Medulla R
2	A+L	Ipsi	No	Ipsi	Contra	No	Saccadic pursuit to L, hypometric saccades to L	Horner R, dysarthria, hoarseness	Medulla R
3	A+L	Ipsi	No	Ipsi	Contra	No	Gaze evoked nystagmus to R, saccadic pursuit to R+L	Horner R, N. V R, vail paresis R	Medulla R
4	A+L	Ipsi	No	Ipsi	Contra	No	Spontaneous nystagmus to L, canal paresis L	Horner R	Medulla R
5	A+L	Ipsi	No	No	Contra	Ipsi	Saccadic pursuit to R		Medulla R
6	A+L	Ipsi	No	Ipsi	Contra	No	Gaze evoked nystagmus to R+L	Horner R, facial pain R	Medulla R
7	A+L	Ipsi	No	No	Contra	No	Saccadic pursuit to R+L, impaired OKN to R	Horner R, dysarthria, dysphagia	Medulla R
8	A+L	Ipsi	Ipsi	Ipsi	Contra	No	Saccadic pursuit to R+L, impaired OKN to R	Horner R, N. V R	Medulla R
9	A+L	Ipsi	No	No	No	No	—	Horner R, vail paresis R	Medulla R
10	A+L	Ipsi	No	No	No	No	Saccadic pursuit to R+L, impaired OKN to L	Horner L, N. V L	Medulla L
11	A+L	Ipsi	No	No	Contra	Ipsi	Spontaneous nystagmus to L	N. V L, vail paresis L	Medulla L
12	A+L	Ipsi	No	Ipsi	Contra	No	Saccadic pursuit to L	Dysphagia	Medulla L
13	A+L	Ipsi	No	Ipsi	No	No	Saccadic pursuit to R+L	Dysphagia, N. V L	Medulla L
14	A+L	Ipsi	No	Ipsi	Contra	No	Gaze evoked nystagmus to R, saccadic pursuit to R+L, hypometric saccades to R	Horner L, dysphagia, N. V L	Medulla L
15	A+L	Ipsi	No	Ipsi	Contra	No	Saccadic pursuit to R+L, impaired OKN to R+L	Horner L, dysarthria, vail paresis L	Medulla L
16	A+L	Ipsi	No	Ipsi	Contra	Ipsi	Gaze evoked nystagmus to R, glissadic saccades to R	Horner L, N. V L, dysarthria	Medulla L
17	A	Ipsi	No	Ipsi	Contra	No	Spontaneous nystagmus to R	Horner L, N. VII L, N. XII L	Medulla L
18	A+L	Ipsi	No	Ipsi	Contra	No	Skew deviation, gaze evoked nystagmus to R+L	Dysarthria, dysphagia	Medulla L
19	A+L	Ipsi	No	Ipsi	Contra	No	Gaze evoked nystagmus to L	Horner L, dysarthria, dysphagia	Medulla L
20	A+L	Ipsi	No	No	Contra	No	—		Medulla L
21	A	Ipsi	No	Ipsi	Contra	No	Saccadic pursuit to R+L	Horner L, dysarthria, dysphagia	Medulla L
22	A+L	Ipsi	No	No	Contra	No	Gaze evoked nystagmus to R, saccadic pursuit to R+L	Dysarthria, N. VII L	Medulla L
23	L	Ipsi	Ipsi	No	No	No	Saccadic pursuit to R+L, impaired OKN to R		Pontomed R
24	A+L	Ipsi	No	Ipsi	No	No	Saccadic pursuit to R+L	N. VII R	Pontomed R
25	A+L	Ipsi	No	Ipsi	Contra	No	—	N. V L	Pontomed L
26	A+L	Ipsi	No	Ipsi	No	No	Spontaneous nystagmus to R	N. V L	Pontomed L
27	A+L	Ipsi	No	Ipsi	No	No	Saccadic pursuit to R+L, impaired fixation suppression to caloric stimulation R+L	N. V L, N. VII L	Pontomed L
28	A+L	Ipsi	No	No	Contra	No	—	N. V R	Pons R
29	A+L	Ipsi	No	Ipsi	No	No	Gaze evoked nystagmus to R+L	N. V R	Pons R
30	A+L	Ipsi	No	No	No	No		N. V R	Pons R
31	A+L	Contra	No	No	No	No	Saccadic pursuit to R+L	N. V R	Pons R
32	A+L	Contra	No	No	No	No	—	Dysarthria	Pons R
33	A+L	Contra	Contra	No	No	No	Glissadic saccades to R, saccadic pursuit to R+L		Pons R
34	A+L	Contra	Contra	No	No	No	Glissadic saccades to L, saccadic pursuit to R+L, impaired OKN to R+L	Dysarthria	Pons L
35	A+L	Contra	Contra	No	No	No	Saccadic pursuit to R, impaired OKN to R	Dysarthria	Pons L
36	A+L	Contra	No	No	No	No	—		Pons L
37	A+L	Contra	Contra	No	No	No	INO L	Ptosis L	Pons L
38	A+L	Contra	Contra	Contra	No	Contra	Gaze evoked nystagmus to R+L	Horner L, N. V L	Pons L
39	A+L	Contra	Contra	Contra	No	No	Impaired fixation suppression to caloric stimulation R+L	Dysarthria	Pons L
40	A+L	Contra	Contra	No	No	No	Saccadic pursuit to R+L	Dysarthria, dysphagia	Pons L

(continued on next page)

Table 1 (continued)

No.	Limb	Ataxia	Hemip	Latero	Pain/Temperature	Touch	Ocular motor disorders	Others	Lesion
41	A+L	Contra	No	Contra	No	No	N. III R		Pontomes R
42	A+L	Both	No	No	No	No	Saccadic pursuit to R, impaired OKN to R+L		Medulla R
43	A+L	Both	No	Contra	No	No	Skew deviation, gaze evoked nystagmus to L	Dysarthria	Pons R
44	A+L	Both	No	Contra	No	No	—		Pons R
45	A+L	Both	Contra	No	No	No	Abduction deficit left eye		Pons L
46	A+L	Both	No	No	Contra	No	Skew deviation	Dysarthria, N. V L	Pons L
47	A+L	Both	No	Contra	No	No	Skew deviation, INO R		Pons R
48	A+L	Both	No	No	No	No	INO R	Dysarthria	Pontomes R
49	A+L	Both	No	No	No	No	INO R+L		Pontomes L

Clinical characteristics of the patient cohort.

The table shows affected limb, side of ataxia, hemiparesis, lateropulsion, and sensory impairment for pain/temperature and touch with regard to the side of brain stem lesion. Ocular motor disorders as to clinical and electrooculographical investigations and further clinical signs are listed.

Abbreviations: Hemip: hemiparesis, Latero: Lateropulsion, A: arm, L: leg, Ipsi: ipsilateral to the brain stem lesion, Contra: contralateral, R: right, L: left, OKN: optokinetic nystagmus, INO: internuclear ophthalmoplegia, N. III: oculomotor nerve paresis, N. V: trigeminal sensory deficit, N. VII: facial nerve paresis, N. XII: hypoglossal nerve paresis, Pontomed: pontomedullary, Pontomes: pontomesencaphalic.

EPI-diffusion-weighted (DWI) images were also collected within 48 h after the onset of symptoms, using DWI-echo planar imaging (TR 4000 ms, TE 103 ms) with separately applied diffusion gradients in the three spatial axes ( $b=1164 \text{ s/mm}^3$ , 128 matrix, 250 ms per slice, 20 slices, thickness 3 mm, 8 measurements). The area of infarction was identified independently by two neuroradiologists and one neurologist. Corresponding lesions had to be documented on DWI and T2-weighted imaging. We used DWI to prove the acuity of a lesion and high-resolution and T2-weighted MRI to outline the extension of the lesion.

#### Three-dimensional mapping and statistics

The manually outlined image was zoomed, scaled, rotated, and non-linearly warped in three dimensions, to be imported and normalised in the brain stem model according to the brainstem outlines and anatomical landmarks like the forth ventricle or the exit zones of cranial nerves (Fig. 1B/C). This is a voxel-based three-dimensional model (Capozza et al., 2000) developed using

data from several topometric and stereotactic atlases (Schaltenbrand and Wahren, 1977; Paxinos and Huang, 1995; Kretschmann and Weinrich, 1998). It is subdivided into 5268 volume elements (“voxels”) ranging from  $2 \times 2 \times 2 \text{ mm}$  to  $2 \times 2 \times 4 \text{ mm}$ . After MR images were imported, to each voxel of the brainstem was assigned a value of 0, 0.5 or 1; a value of 1 represented a voxel certainly affected by the lesion, a value of 0 represented a voxel certainly unaffected, and a value of 0.5 stood for a voxel only partly affected by the lesion. Statistical analysis of patient groups aimed at identifying which voxels out of the 5268 were significantly affected. The system used  $\chi^2$  or Kolmogorov-Smirnov tests in order to perform a within-group, one-sample analysis. In this case, for each voxel the statistical probabilities of finding an affected voxel in the patient group were calculated against a hypothetical mean value for the probability of finding a chance lesion, provided by the average number of affected voxels in the whole population (patients with and without limb ataxia).

For two-sample statistical analysis between two patient groups we used Mann-Whitney  $U$  test. The statistical significance was

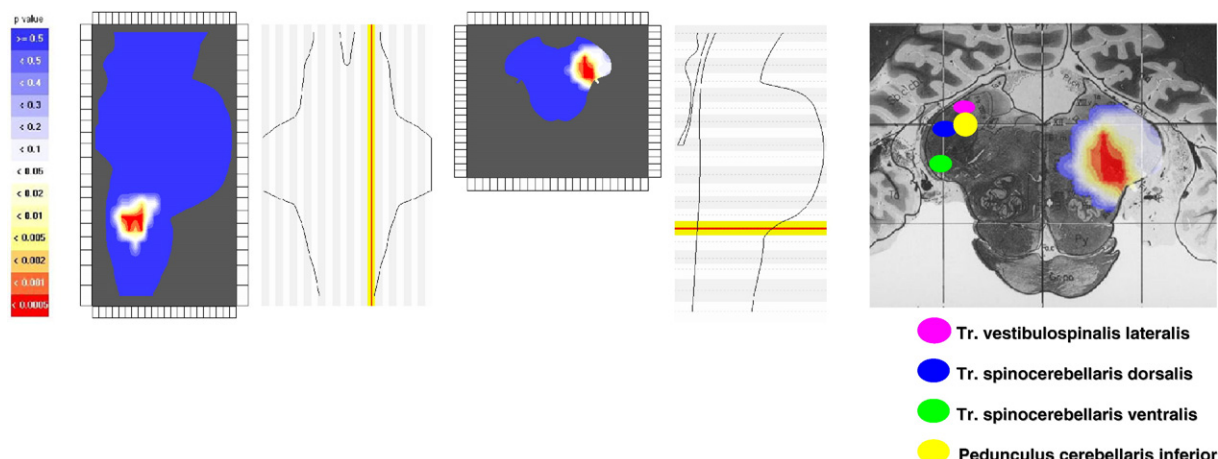


Fig. 2. Colour-coded probability maps on the 3D brainstem model and projection on the corresponding transversal slices of the anatomical atlas of Schaltenbrand and Wahren (1977) showing significantly affected voxels in 28 patients with hemiataxia ipsilateral to the side of lesion ( $\chi^2$  test).

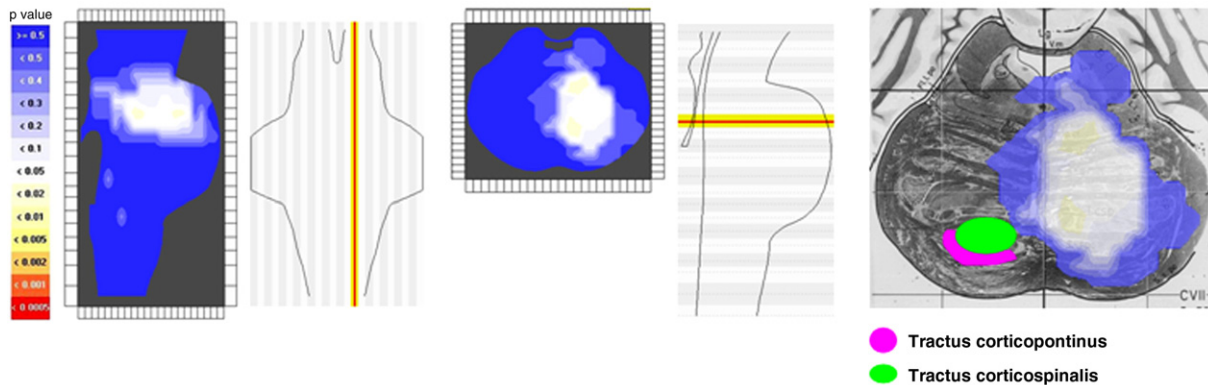


Fig. 3. Colour-coded probability maps on the 3D brainstem model and projection on the corresponding transversal slices of the anatomical atlas of Schaltenbrand and Wahren, 1977 showing significantly affected voxels ( $\chi^2$  test) in 12 patients with hemiataxia and motor hemiparesis contralateral to the side of lesion.

colour coded in each voxel from blue (non-significant), to white (affected with low significance,  $p<0.05$ ), and red (affected with highest significance,  $p<0.0005$ ) with intermediate colours, and displayed at its proper location in the brainstem model. This created a 3D parametric map of the statistical result. From the 3D visualisation, 2D slices can be extracted along any of the three main section planes and be further elaborated to smooth the boundaries.

## Result

### Patient data

Forty-nine of the 362 patients revealed clinical hemiataxia due to isolated acute brain stem infarction documented on MRI. Twenty-six of these patients were recruited at the Department of Neurology, Johannes Gutenberg-University Mainz, Germany, and 23 patients at the Department of Neurological Sciences, La Sapienza University of Rome, Italy. Thirty-three patients were male and 16 were female. Age ranged from 33 to 88 years (mean age 65.8 years). Twenty-three (46.9%) of these patients had medullary, 5 (10.2%) had pontomedullary, 18 (36.7%) had pontine, and three patients (6.1%) had pontomesencephalic infarction.

In 26 patients a complete aetiological diagnostic work up was available. Sonography and MR angiography detected occlusion or stenosis of the vertebral artery in six patients. Sixteen patients had

multiple vascular risk factors and sonography demonstrated macroangiopathy of the internal carotid artery but no vertebral stenosis or occlusion. One patient had vertebral artery dissection following a chiropractic maneuver. In three patients cardioembolic infarction due to atrial fibrillation was the most probable cause of brainstem ischaemia. In six patients of the 26 cases the aetiology of the infarction remained unclear.

Limb ataxia was unilateral in 41 patients (83.7%) and bilateral in eight individuals (16.3%). In 46 patients (93%) limb ataxia involved both arm and leg. Only in three patients (6.1%) that ataxia was restricted to one limb. See Table 1 for detailed clinical data in all patients. Gait ataxia was the predominant accompanying symptom in 75.5% of patients, mainly in combination with body lateropulsion to the side of lesion (53.1%). Signs of vestibular dysfunction were found in seven patients (14.3%). Four of these patients showed a skew deviation, and four patients had spontaneous nystagmus. Of the 26 patients with body lateropulsion only four patients (15.4%) had vestibular signs. Most ocular motor disorders were subclinical and only detected in further electro-oculographical recordings. The most frequent abnormalities were disturbed and saccadic smooth pursuit (44.9%), gaze evoked nystagmus (22.4%) and impaired optokinetic nystagmus (16.3%).

Motor hemiparesis was clinically present in ten patients (20.5%). Suspected pyramidal tract dysfunction was electrophysiologically verified in all ten patients with corresponding clinical signs.

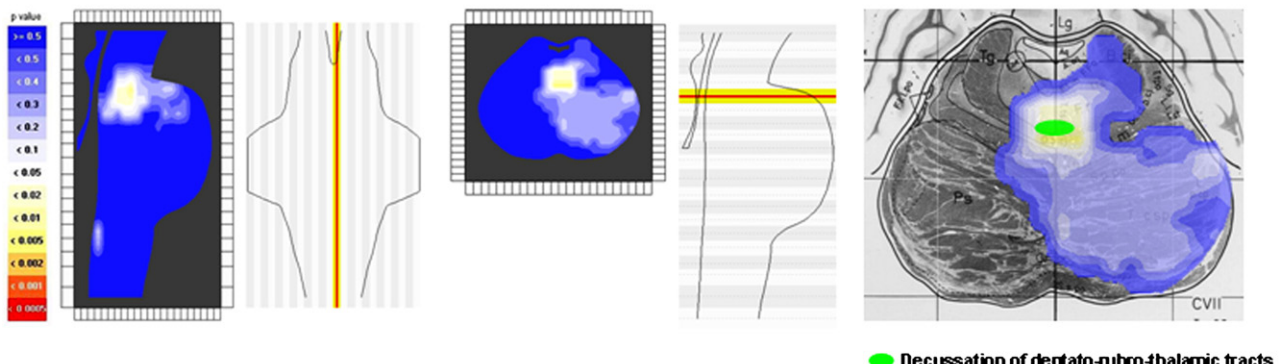


Fig. 4. Colour-coded probability maps on the 3D brainstem model and projection on the corresponding transversal slice of the anatomical atlas of Schaltenbrand and Wahren, 1977 showing significantly affected voxels ( $\chi^2$  test) in 9 patients with bilateral hemiataxia.

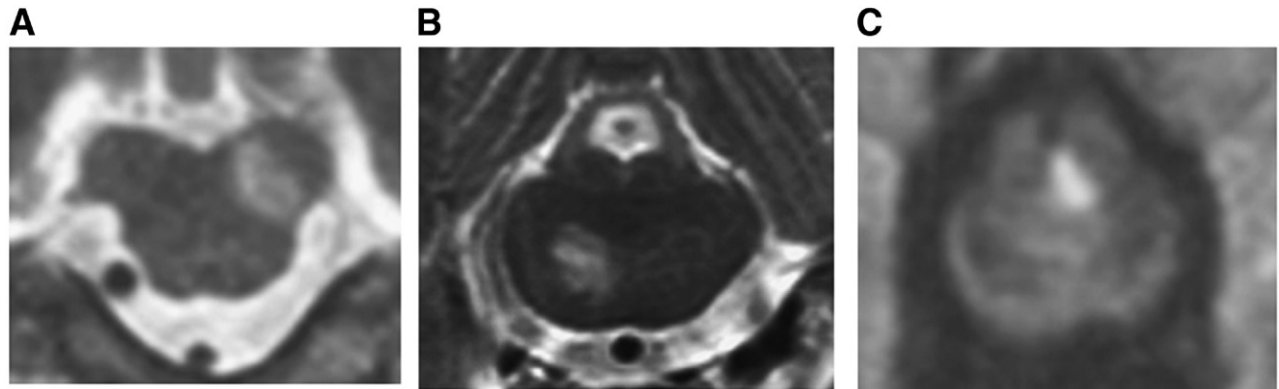


Fig. 5. Axial MRI images showing a typical lesion in (A) patients with medullary infarction and ipsilateral limb ataxia (EPI-T2), (B) in patients with pontine infarction and contralateral limb ataxia (EPI-T2) and (C) in patients with upper central pontine infarction and bilateral limb ataxia (EPI-DWI).

#### Topodiagnostic analysis

One-sample analysis using Kolmogorov–Smirnov test in the 41 patients with unilateral limb ataxia revealed an association of hemiataxia with two different brainstem areas, one with the ipsilateral medulla and the other with the contralateral pons. Two-sample analysis between patients with and without ipsilateral ataxia showed an area of very high probability for ipsilateral ataxia in the dorsal–lateral medulla oblongata ( $p < 0.001$ , Mann–Whitney). In rostral–caudal extension this area was located in the upper medulla oblongata, 27.5–30.0 mm caudal to the pontomesencephalic junction following the transversal slices of the anatomical atlas of Schaltenbrand and Wahren (1977). The area included the ventral and dorsal spinocerebellar tracts and a large portion of the lower cerebellar peduncle; with respect to the vestibular system, it centred slightly ventral and medial to the lateral vestibular nucleus and vestibulospinal tract (Fig. 2). To test for the importance of a vestibular involvement, we also investigated lesion location in patients with hemiataxia plus lateropulsion versus those without lateropulsion. Mann–Whitney  $U$  test revealed an area slightly, but significantly more medial ( $p < 0.01$ ) in patients with additional lateropulsion. The lesion analysis between patients with and without contralateral ataxia depicted an area of moderate significance ( $p < 0.01$ , Mann–Whitney  $U$  test) in the upper pons to be associated with contralateral ataxia (Fig. 3). When additional motor hemiparesis was present on the side of limb ataxia (10 patients) a highly significant correlation appeared with lesions in the contralateral and ventral medial pontine base ( $p < 0.001$ ).

In patients with bilateral ataxia (9 patients) only a weak association was found with an area in the paramedian upper pons and lower midbrain, near to the ventricle base involving the decussation of dentato-rubro-thalamic fibre tracts as depicted in the anatomical atlases ( $p < 0.05$ ) (Fig. 4).

A two-sample analysis comparing patients with limb ataxia solely affecting arm or leg revealed no significant difference in lesion location for the two groups ( $p > 0.1$ ; Mann–Whitney  $U$  test), probably due to the small patient number (3 patients).

#### Discussion

According to this first mapping analysis over the whole human brainstem, clinical hemiataxia may result from at least three distinct brainstem lesions each reflecting a different pathophysiology.

#### Ipsilateral hemiataxia in medullary lesions

Ataxia is caused by lesions of the ipsilateral dorsal–lateral medulla oblongata, especially when hemiataxia is accompanied by contralateral impairment of thermal and pain sensitivity. Limb ataxia is a well-known clinical sign in dorsolateral medullary infarction like typical Wallenberg's syndrome (Fitzek et al., 1999; Kim, 2003). Our mapping analysis revealed that the inferior cerebellar peduncle, and the dorsal and ventral spinocerebellar fibre tracts are the functional structures most likely responsible for this clinical deficit. Lateropulsion and ataxia following brainstem ischaemia have also been described in lesions of the vestibular nuclei and vestibulospinal projections (Grant, 1966; Dieterich and Brandt, 1992). The significantly affected area in our cohort of medullary infarctions was located ventral to the descending vestibulospinal tract, thus arguing against a contribution of the vestibular system to clinical hemiataxia in this situation. Moreover, clinical signs of vestibular dysfunction were extremely rare, even in patients with additional body lateropulsion.

In our patients with unilateral medullary infarction ataxia was ipsilateral rather than bilateral, although the affected ventral spinocerebellar tract is supposed to convey information from both sides (Smith, 1957; Yoss, 1953). According to animal studies in the cat and monkey the ventral spinocerebellar tract conveys incomplete proprioceptive information from the ipsi- and contralateral leg alone, while the dorsal spinocerebellar tract transfers more complete afferent input from the ipsilateral arm and leg (Grant, 1962; Oscarsson, 1973). Given this anatomical preference, lesions of the dorsal spinocerebellar tract may not be fully compensated by the incomplete contralateral proprioceptive information mediated via the intact ventral spinocerebellar tract. Our analysis supports the hypothesis that the spinocerebellar fibre tracts show a corresponding organisation also in humans. This would make an interruption of the dorsal spinocerebellar tract crucial to clinical hemiataxia in lateral medullary lesions. The strongest correlation to lateral medullary lesion was found in patients with additional lateropulsion to the side of limb ataxia. This supports the data of an earlier investigation, where lesions involved the dorsal spinocerebellar tract when body lateropulsion was accompanied by hemiataxia, while pure body lateropulsion was found in more medial medullary infarctions sparing the spinocerebellar tracts but affecting the lateral vestibulospinal tract (Thomke et al., 2005). In medullary infarctions hemiataxia is

frequently accompanied by impairment of contralateral thermal and pain sensitivity reflecting a lesion of ascending spinothalamic and spinoreticular fibres and focussing the lesions to the lateral medulla oblongata (Fitzek et al., 1999; Kim, 2003).

#### *Contralateral hemiataxia in ventral pontine lesions*

Based on our mapping analysis clinical hemiataxia is, however, not exclusively associated with ipsilateral ischaemia. We found a second significant correlation of hemiataxia and contralateral pontine ischaemia. This was even more prominent, when hemiataxia was accompanied by motor paresis. This association is far less frequently reported than hemiataxia following medullary infarction. In part, this may result from the difficulties in assessing limb ataxia in paretic limbs. Dorsolateral medullary infarction usually excludes motor paresis, because the corticospinal fibres descend distantly through the most ventral medulla (Brodal, 1981). Hemiparesis is much more frequent in pontine ischaemia due to the ventral location of the pyramidal tract in the pons, where according to anatomical correlation studies ischaemia is common following occlusion of anteriomedial pontine arteries (*Arteriae paramedianae* of Foix and Hillemand) (Bassetti et al., 1996). The association of hemiataxia and hemiparesis suggests a close proximity of pontine lesions causing hemiataxia to corticospinal projections. It is striking that none of our patients had ipsilateral hemiataxia following pontine ischaemia although the lesions should equally affect pontine nuclei and crossing fibres projecting to the cerebellum. Due to animal studies in the monkey (Schmahmann et al., 2004a), pontocerebellar fibres from one side of the pons traverse the opposite hemipons and disperse amongst numerous widely divergent pontocerebellar fascicles before converging in the opposite brachium pontis and finally entering the cerebellum via the middle cerebellar peduncle. Thus, hemiataxia accompanied by motor paresis may arise from lesions affecting corticopontine and corticospinal fibres that descend close to each other up to the midpontine level. Moreover, direct damage to the pontine neurons itself may result in contralateral impairment (Brodal and Jansen, 1946; King et al., 1968). Smaller lesions do probably not affect a sufficient number of already crossed pontocerebellar fibres, so that a significant amount of neurons may bypass the lesion and thus prevent additional ipsilesional hemiataxia.

#### *Bilateral ataxia in rostral lesions*

Bilateral ataxia is a rare finding in brainstem ischaemia. Our correlation analysis in few patients depicts an area in the paramedian upper pons and lower midbrain, affecting the decussation of both efferent cerebellar dentato-rubro-thalamic fibre tracts as they leave the cerebellum via the upper cerebellar peduncle (Larsell and Jansen, 1972; Flumerfelt et al., 1973). Thus, bilateral ataxia in brainstem ischaemia may again result from a different mechanism than the loss of proprioceptive input or impairment of pontocerebellar connections. It probably represents an interruption of efferent cerebellar outflow especially of the dentate nuclei. The number of patients, however, was too small to check for a predominantly distal motor limb involvement as expected from lesions of the dentato-rubro-thalamic connections (Courville, 1966; Flumerfelt et al., 1973).

It seems unlikely that ataxia is caused by a lesion of the ventral spinocerebellar tracts that cross midline in an adjacent area, because they convey proprioceptive information of the lower limbs

alone and a disruption did not prove to be clinically important in medullary lesions. Moreover, a lesion of the decussation of both ventral spinocerebellar tracts before entering the superior cerebellar peduncles at a rostral pontomesencephalic level should spare both dorsal spinocerebellar tracts, thus preventing clinically apparent ataxia (Fig. 5).

#### *Conclusions*

Ataxia in brainstem ischaemia may have a distinct topodiagnostic value, while different lesion locations each represents a different underlying pathophysiology of the disorder. (1) When hemiataxia is accompanied by contralateral thermal/pain sensitivity impairment it is almost exclusively caused by ipsilateral dorsal-lateral medullary infarction, especially when additional lateropulsion is present. In this case medullary ischaemia involves a slightly more medial medullary brainstem area than classical dorsal-lateral medullary infarction. Here, hemiataxia is supposed to be a consequence of impaired proprioceptive input. (2) In patients with accompanying motor paresis, hemiataxia is a sign of contralateral pontine ischaemia affecting the corticopontine projections or pontine base nuclei of the cortico-ponto-cerebellar pathway. (3) Bilateral ataxia is a rare finding in brainstem ischaemia and probably reflects a lesion of both efferent cerebellar dentato-rubro-thalamic fibre tracts at midline on a central rostral pontine level.

Our understanding of functional brainstem systems is to date incomplete, which is mainly due to the close proximity of brainstem nuclei and fibre tracts making structural-functional correlation studies difficult. So far, functional imaging, like PET or fMRI studies has not convincingly contributed to mapping of brainstem function. Classical functional-structural mapping for *in vivo* mapping is mostly based on a restricted number of samples and thus lacking a quantitative and statistically supported approach. Moreover, there is always a risk for highlighting vascular territories, rather than the structures specifically responsible for the clinical dysfunction when mapping is based on vascular lesions. Our approach is minimising this confounder by statistically comparing lesion location in a sample of stroke patients with and without a given dysfunction. The technique does, however, not completely ignore the vascular architecture of the brain stem. It is impossible to make reliable topographic allocation in brain stem areas that are generally not affected by ischaemia. The technique proved to yield reliable results in mapping analyses of functional systems that do not follow vascular territories like the central reflex loops of several brain stem reflexes (Crucu et al., 2005). Including further inflammatory lesions for mapping analysis is problematic, as these lesions are hardly ever isolated and lesion outlines are difficult to define. In the future, new techniques like tensor weighted imaging using high field scanners may enable tracking even of small fibre tracts in the brain stem. So far, the directionality and the precise location of the many densely packed and crossing fibre tracts in the brain stem are still difficult to identify (Salamon et al., 2005). Another limitation is the need to define regions of interest for a better resolution, which hinders a topographic mapping free of any hypothesis over the whole brain stem (Shiga et al., 2005). Concerning the responsible structures for clinical limb ataxia, there is a need for further studies focussing on eloquent areas in the upper brainstem, especially the mesencephalon. Regarding the overrepresentation of lower brainstem infarctions in our fairly large cohort of patients with brainstem ischaemia this is, however, going to be a challenging task.

## Acknowledgment

The study was supported by the DFG (Deutsche Forschungsgemeinschaft) Ho293/10-1.

## References

- Bassetti, C., Bogousslavsky, J., Barth, A., Regli, F., 1996. Isolated infarcts of the pons. *Neurology* 46, 165–175.
- Brodal, A., 1981. *Neurological Anatomy*, 3rd edition. Oxford Univ. Press, New York.
- Brodal, A., Jansen, J., 1946. The ponto-cerebellar projection in the rabbit and cat. Experimental investigations. *J. Comp. Neurol.* 84, 31–118.
- Brott, T., Adams Jr, H.P., Olinger, C.P., Marler, J.R., Barsan, W.G., Biller, J., Spilker, J., Holleran, R., Eberle, R., Hertzberg, V., Rorick, M., Moomaw, C.J., Walker, M., 1989. Measurements of acute cerebral infarction: a clinical examination scale. *Stroke* 20, 964–970.
- Capozza, M., Iannetti, G.D., Mostarda, M., Cruccu, G., Accornero, N., 2000. Three-dimensional mapping of brainstem functional lesions. *Med. Biol. Eng. Comput.* 38, 1–6.
- Courville, J., 1966. Somatotopical organization of the projections from the nucleus interpositus anterior of the cerebellum to the red nucleus. An experimental study in the cat with silver impregnation methods. *Exp. Brain Res.* 2, 191–215.
- Cruccu, G., Marx, J.J., Iannetti, G.D., Thoemke, F., Truini, A., Fitzek, S., Galeotti, F., Urban, P.P., Romaniello, A., Stoeter, P., Manfredi, M., Hopf, H.C., 2005. Brainstem reflex circuits revisited. *Brain* 128, 386–394.
- Dieterich, M., Brandt, T., 1992. Wallenberg's syndrome: lateropulsion, cyclorotation, and subjective visual vertical in thirty-six patients. *Ann. Neurol.* 31, 399–408.
- Fitzek, S., Fitzek, C., Marx, J., Speckter, H., Urban, P.P., Thomke, F., Stoeter, P., Hopf, H.C., 1999. Blink reflex R2 changes and localisation of lesions in the lower brainstem (Wallenberg's syndrome): an electrophysiological and MRI study. *J. Neurol. Neurosurg. Psychiatry* 67, 630–636.
- Flumerfelt, B.A.S., Otabe, S., Courville, J., 1973. Distinct projections to the red nucleus from the dentate and interposed nuclei in the monkey. *Brain Res.* 50, 408–414.
- Grant, G., 1962. Spinal course and somatotopically localized termination of the spinocerebellar tracts. An experimental study in the cat. *Acta Physiol. Scand.* 56, 1–45 (Suppl.).
- Grant, G., 1962. Infarction localization in a case of Wallenberg's syndrome. A neuroanatomical investigation with comments on structures responsible for nystagmus, impairment of taste and deglutition. *J. Hirnforsch.* 8, 419–430.
- Kim, J.S., 2003. Pure lateral medullary infarction: clinical–radiological correlation of 130 acute, consecutive patients. *Brain* 126, 1864–1872.
- King, J.S., Martin, G.F., Biggert, T., 1968. The basilar pontine grey of the opossum: I. Morphology. *J. Comp. Neurol.* 133, 439–446.
- Kretschmann, H.J., Weinrich, W., 1998. *Neurofunctional Systems—3D Reconstructions With Correlated Neuroimaging*. Thieme, Stuttgart.
- Kumral, E., Bayulkem, G., Evyapan, D., 2002. Clinical spectrum of pontine infarction. Clinical-MRI correlations. *J. Neurol.* 249, 1659–1670.
- Larsell, O., Jansen, J., 1972. *The Comparative Anatomy and Histology of the Cerebellum. The Human Cerebellum, Cerebellar Connections and Cerebellar Cortex*. University of Minnesota Press, Minneapolis.
- Marx, J.J., Iannetti, G.D., Thoemke, F., Fitzek, S., Urban, P.P., Stoeter, P., Cruccu, G., Dieterich, M., Hopf, H.C., 2005. Somatotopic organization of the corticospinal tract in the human brainstem: a MRI-based mapping analysis. *Ann. Neurol.* 57, 824–831.
- Oscarsson, O., 1973. Functional organization of spinocerebellar paths. In: Iggo, A. (Ed.), *Handbook of Sensory Physiology. Somatosensory System*, vol. II. Springer, Berlin, pp. 339–380.
- Paxinos, G., Huang, X.F., 1995. *Atlas of the Human Brainstem*. San Diego Academic Press, San Diego.
- Rondot, P., 1969. Motor function. In: Vinkin, P.J., Bruyn, G.W. (Eds.), *Handbook of Clinical Neurology*, vol 1. North-Holland, Amsterdam, pp. 147–168.
- Sacco, R.L., Freddo, L., Bello, J.A., Odel, J.G., Onesti, S.T., Mohr, J.P., 1993. Wallenberg's lateral medullary syndrome. Clinical-magnetic resonance imaging correlations. *Arch. Neurol.* 50, 609–614.
- Salamon, N., Sicotte, N., Alger, J., Shattuck, D., Perlman, S., Sinha, U., Schultze-Haakh, H., Salamon, G., 2005. Analysis of the brain-stem white-matter tracts with diffusion tensor imaging. *Neuroradiology* 47, 895–902.
- Schaltenbrand, G., Wahren, W., 1977. *Atlas for Stereotaxy of the Human Brain*. Thieme, Stuttgart.
- Schmahmann, J.D., Rosene, D.L., Pandya, D.N., 2004a. Ataxia after pontine stroke: insights from pontocerebellar fibers in monkey. *Ann. Neurol.* 55, 585–589.
- Schmahmann, J.D., Ko, R., MacMore, J., 2004b. The human basis pontis: motor syndromes and topographic organization. *Brain* 127, 1269–1291.
- Shiga, K., Yamada, K., Yoshikawa, K., Mizuno, T., Nishimura, T., Nakagawa, M., 2005. Local tissue anisotropy decreases in cerebellopetal fibers and pyramidal tract in multiple system atrophy. *J. Neurol.* 252, 589–596.
- Smith, M.C., 1957. The anatomy of the spino-cerebellar fibres in man: I. The course of the fibers in the spinal cord and brain stem. *J. Comp. Neurol.* 108, 285–352.
- Thomke, F., Marx, J.J., Iannetti, G.D., Cruccu, G., Fitzek, S., Urban, P.P., Stoeter, P., Cruccu, G., Dieterich, M., Hopf, H.C., 2005. A topodiagnostic investigation on body lateropulsion in medullary infarcts. *Neurology* 64, 716–718.
- Trouillas, P., Takayanagi, T., Hallett, M., Currier, R.D., Subramony, S.H., Wessel, K., Bryer, A., Diener, H.C., Massaquoi, S., Gomez, C.M., Coutinho, P., Ben Hamida, M., Campanella, G., Filla, A., Schut, L., Timann, D., Honnorat, J., Nighoghossian, N., Manyam, B., 1997. International Cooperative Ataxia Rating Scale for pharmacological assessment of the cerebellar syndrome. The Ataxia Neuropharmacology Committee of the World Federation of Neurology. *J. Neurol. Sci.* 145, 205–211.
- Urban, P.P., Hopf, H.C., Zorowka, P.G., Fleischer, S., Andereas, J., 1996. Dysarthria and lacunar stroke pathophysiological aspects. *Neurology* 47, 1135–1141.
- Urban, P.P., Wicht, S., Vucoevic, G., Fitzek, S., Marx, J., Thomke, F., Mika-Gruttner, A., Fitzek, C., Stoeter, P., Hopf, H.C., 2001. The course of corticofacial projections in the human brainstem. *Brain* 124, 1866–1876.
- Yoss, R.E., 1953. Studies of the spinal cord: Part II. Topographic localization within the dorsal spino-cerebellar tract in the macaque. *J. Comp. Neurol.* 99, 613–638.